Quantum recoil in free-electron interactions with atomic lattices

Huang, Sunchao; Duan, Ruihuan; Pramanik, Nikhil; Herrin, Jason Scott; Boothroyd, Chris; Liu, Zheng; Wong, Liang Jie

2023

Huang, S., Duan, R., Pramanik, N., Herrin, J. S., Boothroyd, C., Liu, Z. & Wong, L. J. (2023). Quantum recoil in free-electron interactions with atomic lattices. Nature Photonics. https://dx.doi.org/10.1038/s41566-022-01132-6

https://hdl.handle.net/10356/164440

https://doi.org/10.1038/s41566-022-01132-6

Quantum recoil in free electron interaction with atomic lattices

Sunchao Huang[1], Ruihuan Duan[2], Nikhil Pramanik[1], Jason Scott Herrin[3,4], Chris Boothroyd[4,5], Zheng Liu[5] and Liang Jie Wong[1⋆]

[1]*School of Electrical and Electronic Engineering, Nanyang Technological University, 50 Nanyang Avenue, Singapore 639798, Singapore*

[2]*CINTRA CNRS/NTU/THALES, UMI 3288, Research Techno Plaza, Nanyang Technological University, 50 Nanyang Avenue, Singapore 637371, Singapore*

[3]*Earth Observatory of Singapore, Nanyang Technological University, 50 Nanyang Avenue, Singapore 639798, Singapore*

[4]*Facility for Analysis, Characterisation, Testing and Simulation (FACTS), Nanyang Technological University, 50 Nanyang Avenue, Singapore 639798, Singapore*

[5]School of Materials Science and Engineering, Nanyang Technological University, 50 Nanyang Avenue, Singapore 639798, Singapore

⋆Email: liangjie.wong@ntu.edu.sg

The emission of light from charged particles underlies a wealth of scientific phenomena and technological applications. Classical theory determines the emitted photon energy by assuming an undeflected charged particle trajectory. In 1940, Ginzburg pointed out that this assumption breaks down in quantum electrodynamics, resulting in shifts – known as quantum recoil – in outgoing photon energies from their classically predicted values. Since then, quantum recoil in free electron light emission processes, including Cherenkov radiation and Smith-Purcell radiation, has been well-studied in theory, but an experimental demonstration has remained elusive. Here, we present an experimental demonstration of quantum recoil, showing that this quantum electrodynamical effect is not only observable at room temperature, but also robust in the presence of other electron scattering mechanisms. By scattering free electrons off the periodic 2D atomic sheets of van der Waals materials in a table-top platform, we show that the x-ray photon energy is accurately predicted only by quantum recoil theory. We show that quantum recoil can be enormous: to the point that a classically predicted x-ray photon is emitted as an arbitrarily low energy photon. We envisage quantum recoil as a means of precision control over outgoing photon and electron spectra, and show

that quantum recoil can be tailored through a host of parameters: the electron energy, the atomic composition and tilt angle of the van der Waals material. Our results pave the way to table-top, room-temperature platforms for harnessing and investigating quantum electrodynamical effects in electron-photon interactions.

Free electron spontaneous emission phenomena, such as the Smith-Purcell effect [1, 2] and Cherenkov radiation [3, 4], have driven a wide range of technological innovations and scientific discoveries [5–19]. In the Smith-Purcell effect, photons are emitted when the Coulomb field of an electron scatters off a periodic structure as the electron travels in constant motion near or through it. The Smith-Purcell effect has been investigated as a tunable light source in many regimes of the electromagnetic spectrum, from microwave to x-ray frequencies [19–22]. Additionally, the Smith-Purcell effect has been leveraged for particle identification [13, 14], particle acceleration [23], and the discovery of fundamental radiation limits [10, 24].

Classical theory predicts that the deceleration of the incident electron upon photon emission has a negligible effect in Smith-Purcell radiation. As such, the emitted photon energies predicted by classical theory is a first-order approximation that does not take into consideration energy-momentum conservation enforced by quantum electrodynamics. As pointed out theoretically by Ginzburg in 1940 [25], energy-momentum conservation results in quantum recoil – namely, shifts in the emitted photon energies from the classically predicted values. Furthermore, the emitted photon energies are no longer evenly spaced (i.e., no longer integer multiples of some fundamental harmonic), as is the case in classical theory.

Here, we experimentally demonstrate quantum recoil. In particular, we theoretically predict and experimentally measure quantum recoil in Smith-Purcell radiation using electrons of kinetic energies 11-13 keV from a scanning electron microscope (SEM). The platform is therefore lab-scale, with no external light sources involved. The electrons scatter off the sub-nanometer periodic gratings furnished by the multilayer 2D atomic sheets in van der Waals materials like graphite and hexagonal boron nitride. We are able to observe measurable photon energy shifts in the emitted photons. These experimental measurements confirm the accuracy and importance of quantum recoil theory. We show that quantum recoil can be tailored by controlling the electron energy, the target material's atomic composition and tilt angle, and the emission order. We show that the versatility of quantum recoil allows a classically predicted soft x-ray photon to manifest as a low-energy photon through precision control of the electron and material parameters. We conclude that quantum recoil can be significant even when driven by conventional table-top electron sources at room temperature, and in the presence of other electron scattering events. Even more broadly, our results suggest that the combination of existing

table-top electron sources and crystalline materials is a promising platform for studying related fundamental phenomena, including open questions like radiation reaction [26] and intriguing concepts like the quantum free electron laser [27,28]. Our results also highlight the importance of taking quantum recoil into account when modeling free-electron-driven material systems, such as van der Waals based x-ray emitters [21,22] and other coherent x-ray sources [29–32].

Results

Free electrons impinging on a crystalline solid (Fig. 1a) emit radiation via two mechanisms: the scattering of the free electron Coulomb fields off the periodic lattice, known as parametric x-ray radiation [31,32]; and the acceleration of the free electrons in the crystal's electrostatic potential, known as coherent bremsstrahlung [30–33]. Parametric x-ray radiation, the dominant mechanism in our regime of study, is physically equivalent to the Smith-Purcell effect [2], with the atomic lattice planes playing the role of the periodic grating. In the classical picture where quantum recoil is ignored, the momentum of the electron is assumed to be unchanged upon photon emission, and the output photon angular frequency is given by (e.g., [30])

$$\omega_c = -\frac{c\boldsymbol{g}\cdot\boldsymbol{\beta}}{1-n\boldsymbol{\beta}\cdot\hat{\boldsymbol{q}}}, \tag{1}$$

where c is the speed of light in free space, $\boldsymbol{g}$ is the reciprocal lattice vector (whose magnitude is g), $\boldsymbol{\beta} \equiv \boldsymbol{v}/c$ is the normalized electron velocity, n is the refractive index of the medium, and $\hat{\boldsymbol{q}} = (\sin\theta_{\text{obs}}\cos\phi_{\text{obs}}, \sin\theta_{\text{obs}}\sin\phi_{\text{obs}}, \cos\theta_{\text{obs}})$ is the unit vector of the emitted photon wave vector (θ_{obs} and ϕ_{obs} are the polar and azimuthal angle of $\hat{\boldsymbol{q}}$, respectively). In many cases, even up to recent times, equation (1) has been shown to be adequate in explaining experimental observations [20,22,34,35].

As early as 1940, however, Vitaly L. Ginzburg pointed out theoretically that the above consideration alone cannot describe free electron spontaneous emission with full accuracy [25]. This is because the classical picture ignores quantum recoil, which refers specifically to the $\hbar$-dependent photon energy shift resulting from the electron's reaction upon spontaneously emitting the photon in question (Fig. 1b). Quantum recoil is therefore completely different from – and highly complementary to – other types of recoil, such as those associated with the deflection of electrons by external fields [7,36,37], and the deflection of electrons by scattering events before and after the spontaneous emission event in question [36,38]. Ginzburg's theory has since been expanded by others in the context of Cherenkov radiation and Smith-Purcell ra-

diation [25,39–42]. By applying energy-momentum conservation to our Smith-Purcell scenario, we obtain the output photon angular frequency as

$$\omega = -\frac{2c\boldsymbol{g}\cdot\boldsymbol{\beta} + \hbar c^2 g^2/E_i}{(1 - n\boldsymbol{\beta}\cdot\hat{\boldsymbol{q}} - n\hbar c\boldsymbol{g}\cdot\hat{\boldsymbol{q}}/E_i)\left(1 + \sqrt{1 - \frac{n^2-1}{n^2}\frac{\hbar^2c^2g^2 + 2\hbar cE_i\boldsymbol{g}\cdot\boldsymbol{\beta}}{[E_i(\boldsymbol{\beta}\cdot\hat{\boldsymbol{q}} - 1/n) + \hbar c\boldsymbol{g}\cdot\hat{\boldsymbol{q}}]^2}}\right)}, \tag{2}$$

where E_i is the total energy (i.e., including rest mass) of the incident electron. Equation (2) reduces to the classical equation (1) when the reduced Planck's constant $\hbar$ is artificially set to 0. The parts containing $\hbar$ thus constitute deviations from the classical prediction of equation (1). Indeed, the quantum nature of quantum recoil can be seen from its dependence on $\hbar$, widely regarded as the signature of quantum mechanics. We note that the appearance of $\hbar$ in equation (2) is not due to the quantization of photon energy and momentum (i.e., the de Broglie relations), but instead due to energy-momentum conservation in a quantum electrodynamical process. We point out that a similar result to equation (2) was obtained in [39], but for the specific cases of 1D and 2D nanogratings. It can be shown that equation (2) agrees with the result in [39] under those specialized conditions. The refractive index in the x-ray range can be modeled as $n = 1 - \frac{\omega_p^2}{2\omega^2} \approx 1$, where ω_p is the plasma frequency, using the Lorentz oscillator model. We therefore simplify equation (2) to

$$\omega \approx -\frac{c\boldsymbol{g}\cdot\boldsymbol{\beta} + \hbar c^2 g^2/(2E_i)}{1 - \boldsymbol{\beta}\cdot\hat{\boldsymbol{q}} - \hbar c\boldsymbol{g}\cdot\hat{\boldsymbol{q}}/E_i}. \tag{3}$$

In the limit where quantum recoil is small, we can Taylor expand equation (3) to obtain

$$\omega \approx -\frac{c\boldsymbol{g}\cdot\boldsymbol{\beta}}{1 - \boldsymbol{\beta}\cdot\hat{\boldsymbol{q}}} + \hbar\frac{c^2\boldsymbol{g}\cdot\hat{\boldsymbol{q}}(\boldsymbol{g}\cdot\boldsymbol{\beta})/E_i + c^2g^2(1 - \boldsymbol{\beta}\cdot\hat{\boldsymbol{q}})/(2E_i)}{(1 - \boldsymbol{\beta}\cdot\hat{\boldsymbol{q}})^2}, \tag{4}$$

where the presence of $\hbar$ in the second term indicate the quantum nature of the quantum recoil correction. In many cases, however, quantum recoil is substantial and equation (3) cannot be simplified in this way. We show below that there are conditions under which quantum recoil can be so large that a classically predicted x-ray photon is in fact emitted as a low energy

photon. Details of the derivations are given in Supplementary Information (SI) Section S1. The experiments are performed in a SEM setup, where electrons of kinetic energy 10-15 keV impinge on single-crystal van der Waals materials placed in the sample holder (see Methods). The van der Waals material – graphite in the case of Fig. 1 – is oriented such that the electron travels roughly parallel to the [001] direction. The grating vector $\boldsymbol{g}$ is thus given by

$$\boldsymbol{g}_{(00\bar{m})} = -m\frac{2\pi}{d}(\sin\theta_{\text{til}}\cos\phi_{\text{til}}, \sin\theta_{\text{til}}\sin\phi_{\text{til}}, \cos\theta_{\text{til}}), \tag{5}$$

where m is an integer denoting the order of Smith-Purcell radiation, d is the interlayer distance of the (001) planes, and θ_{til} and ϕ_{til} respectively denote the polar and azimuthal angles of the [001] zone axis relative to the initial direction of electron travel (see Fig. 1c inset). For hexagonal crystals such as graphite and hexagonal boron nitride, emission at odd m is forbidden since the structure factor is zero (see SI Section S2).

An electron traveling through the crystalline van der Waals material will also experience elastic and inelastic scattering beyond Smith-Purcell radiation. To account for the impact of these scattering events, we perform Monte Carlo simulations to determine the changes in velocity of each electron as it travels through the sample material. Between two adjacent scattering events, the Smith-Purcell radiation spectrum can be determined from equations (1, 3, 5). The Smith-Purcell emission from an electron traveling distance L between two adjacent scattering events has a bandwidth

$$\Delta\omega \approx \sqrt{\left(5.6\frac{\beta c}{L}\right)^2 + \left(\frac{\partial\omega}{\partial\theta_{\text{obs}}}\Delta\theta_{\text{obs}}\right)^2 + \Delta\omega_{\text{EDS}}}, \tag{6}$$

where ω is the output photon angular frequency (set to ω_c for the classical case, i.e., equation (1)). The first term (under the square root) in equation (6) corresponds to the intrinsic bandwidth, which is around 20 eV in our case. The second term accounts for the finite range of observation directions admitted by the angular aperture of the x-ray detector. The final term accounts for the energy resolution of the x-ray detector, where $\hbar\Delta\omega_{\text{EDS}} \approx 52$ eV (72 eV) for photon energies around 650 eV (1300 eV). The detector energy resolution thus dominates the total bandwidth in our experiments. The total radiation spectrum is obtained by summing over

all radiation spectra between any two adjacent scatterings contributed by all incident electrons. Broadening of the x-ray emission peaks due to electron scattering and electron beam divergence are thus taken into account via the Monte Carlo simulations. More details on the Monte Carlo simulations are given in the Methods and SI Section S3.

Fig. 1c shows the multimode x-ray spectrum generated by an 11.7 keV electron beam impinging on a graphite single crystal. The filled red circles are experimental results. The blue and green lines are theoretical results corresponding to the classical (equation (1)) and quantum (equation (3)) models respectively, at observation angle $\theta_{\text{obs}} = 130°$, and van der Waals material tilt angles $\theta_{\text{til}} = 12.45°$ and $\phi_{\text{til}} = 0.3°$. The x-ray spectrum contains two distinct photon energy peaks, corresponding to second-order ($m = 2$) and fourth-order ($m = 4$) Smith-Purcell photons. The experimental results are in excellent agreement with quantum theory, and show noticeable discrepancies from the predictions of classical theory. The full x-ray spectrum, details of the multi-Gaussian peak deconvolution and background subtraction yielding the data presented in Fig. 1c, are given in SI Section S4. The details of x-ray detector calibration are given in SI Section S5.

As another way of analyzing the photon energy shift induced by quantum recoil, we consider the energy difference between the second-order ($\hbar\omega_2$) and fourth-order ($\hbar\omega_4$) emission peaks. In the classical picture, equation (1) yields $2\hbar\omega_2 - \hbar\omega_4 = 0$, independent of all parameters including θ_{til} and electron energy. Equation (3), which includes the effects of quantum recoil, shows that the difference generally takes on a non-zero value that depends on the choice of experimental parameters. The experimental results (Fig. 1d) are indicated by the filled red circles, with error bars determined by Gaussian fitting of the measured Smith-Purcell peaks. The good agreement between the experimental results and the quantum theoretical predictions confirms that quantum recoil is indeed measurable using a combination of table-top electron sources and crystalline materials. In this case, electron energies between 10–15 keV were used. Both the classical and quantum predictions have taken electron scattering events beyond Smith-Purcell radiation into consideration by Monte Carlo simulations. Similar results for 55 nm-thick graphite and 95 nm-thick hexagonal boron nitride are shown in SI Section S6, giving further evidence that our quantum recoil measurements and conclusions are robust to material choice and sample thickness. The good agreement between experimental results and quantum theory also affirms that quantum recoil is robust to the presence of other scattering events even in thick samples. Our results constitute an unprecedented measurement of quantum recoil in free electron spontaneous emission. Importantly, they also constitute the observation of a quantum phenomenon at room-temperature, while requiring only a table-top source of free electrons.

In our experiments, hexagonal boron nitride and graphite thin films are mechanically exfoliated from their bulk counterparts, and transferred to Au grids with the aid of the wet-transfer method. The surface of these thin film are (001) planes. The tilt angles θ_{til} and ϕ_{til}, the polar and azimuthal angles of the [001] zone axis, are usually not zero since the Au grid is not atomically flat. Furthermore, some areas of the sample are bent during the sample preparation and/or the during the loading of the Au grid to the sample holder of the SEM. The sample tilt angles can be accurately determined in transmission electron microscopes with Kikuchi line [22], where the value of θ_{til} is within 10 degrees and the value of ϕ_{til} can be any value from 0 to 2π. However, this only gives us an estimate of the actual sample tilt angles in the SEM. To accurately determine the sample tilt angles in the SEMs itself, we perform a fitting for them by matching the measured peak photon energies with theoretical predictions. To ensure this does *not* unfairly favor our hypothesis that the experiment should match quantum theory, we use the classical equations to fit the experimental data for the classical theory predictions, and we use the quantum equations to fit the experimental data for the quantum theory predictions. Importantly, we find that only the results of quantum theory agree with experimental measurements (e.g. Fig. 1d), with the least squares error of the fitting being over 10 times superior for the quantum case than for the classical case. The uncertainty associated with the fittings is also included in the error bars of Fig. 1d. More details are described in the Methods and SI Section S7.

The x-ray spectra (compared against classical and quantum predictions) corresponding to various points in Fig. 1d are shown in Figs. 2a-c. Figs. 2d-f shows results obtained from hexagonal boron nitride (the figure corresponding to Fig. 1d for this set of measurements is presented in SI Section S6). In all cases, we see that the experimental measurements confirm the importance of taking quantum recoil into account when predicting the photon energy output from Smith-Purcell radiation.

To give an idea of the x-ray intensity generated by our experiments, the measured x-ray intensity is about 0.012 pW for the second-order x-rays, and 0.004 pW for the fourth-order x-rays in Fig. 2f. These measurements were performed using an average of current of about 4.4 nA at an observation angle of $119.0° \pm 5.5°$. The corresponding photon flux is 3.4×10^3 photons/(s·sr) for second-order x-rays, and 5.0×10^2 photons/(s·sr) for fourth-order x-rays. In units of photons/(electron.sr), this corresponds to 1.2×10^{-7} photons/(electron·sr) for the second-order x-rays, and 1.8×10^{-8} photons/(electron·sr) for the fourth-order x-rays. Note that these estimates of intensity and photon flux only include the photons detected by the employed setup, and not the photons emitted at all angles. Although the main purpose of our study

is not to demonstrate a commercially ready source of x-rays, we note that by scaling up the current up to 5 mA, typical in conventional x-ray tubes, we achieve an x-ray flux of about 3.8×10^9 photons/(s·sr) for second order x-rays and about 5.6×10^8 photons/(s·sr) for fourth-order x-rays. If we take the distance between the x-ray source and an x-ray imaging detector (e.g., a charge-coupled device) to be 10 cm, the corresponding x-ray intensity at the detector is 3.8×10^5 photons/(s·mm^2) for second order x-rays and about 5.6×10^4 photons/(s·mm^2) for fourth-order x-rays. Such x-ray intensities have been shown to be adequate for imaging applications for sufficiently thin samples [43].

Due to energy conservation, quantum recoil not only induces energy shifts in the emitted photons, but also affects the quantized energy loss in the outgoing electrons. The emitted photon energy and the corresponding electron energy loss are entangled via energy conservation, potentially also allowing us to observe quantum recoil by measuring the post-selected electron energy loss spectrum (see SI Section S8 for details). In particular, measuring the post-selected electron energy loss spectrum would involve recording the outgoing electron energies if and only if outgoing photons corresponding to the shifted photon energy peaks are simultaneously detected. This is more cumbersome than (but equivalent to) directly measuring the outgoing photon energy shifts, as we have done in this work. It should also be noted that this post-selected electron energy loss spectrum would feature peaks that are shifted as compared to the peaks predicted by classical theory. Therefore, simply measuring the quantized energy loss of the electrons does not constitute an observation of quantum recoil, unless the presence of quantum recoil-induced energy shifts can be verified. Our success in measuring quantum recoil in Smith-Purcell radiation motivates the investigation of similar quantum mechanical effects in inverse processes where optical waveforms are used to control or accelerate electrons [18,23,37].

Fig. 3 illustrates the tuning of quantum recoil via various degrees of freedom. We see that a wide range of quantum recoil tuning can be achieved even by confining ourselves to table-top electron energies: from practically zero quantum recoil, to quantum recoil so strong that a classically predicted soft x-ray photon emerges as an extremely low energy photon. The tuning can be performed by varying the electron kinetic energy and material tilt angle; by changing the atomic composition of the target material; or by measuring radiation emission of different orders m, where m refers to radiation corresponding to the $(00\bar{m})$ reciprocal lattice vector. Although Fig. 3 considers the specific case of a classically predicted 300 eV photon, the same principles and conclusions would apply to photons of other energies (see SI Section S9 for examples of other classically predicted photons energies). Here, multiple values of interlayer spacing d are used for graphite to reflect the fact that its interlayer spacing can be tuned

by controlling the conditions of its synthesis [44], giving us flexibility even with one type of material. Importantly, our findings indicate that conventional table-top electron sources of kinetic energies 1-300 keV (which include SEM and TEM energies), in combination with crystalline materials, are promising platforms to investigate quantum recoil in free electron spontaneous emission.

Discussion

We have shown that quantum recoil in free electron spontaneous emission can be measured and tuned in a lab-scale platform. This platform is useful for exploring new phenomena as well as realizing intriguing science in the regime of substantial quantum recoil. Our findings directly corroborate effects arising in light-matter interaction due to quantization of the electromagnetic field. These effects were first analyzed in the context of Cherenkov radiation by Ginzburg and Sokolov [25, 40], and have been predicted to cause quantum recoil in free electron spontaneous emission [39, 42]. Our findings provide unprecedented experimental confirmation of quantum recoil in the context of the Smith-Purcell effect. This shows that a table-top platform can already provide important headway into these studies. Together with higher-order quantum electrodynamics processes [45] and the quantum-wave nature of the electron (e.g., arising from shaping the electron wavefunction spatially and temporally) [42, 46–48], measuring quantum recoil paves the way to studying fundamental physics and potential technological advances arising from quantum aspects of electron-photon interactions [49].

Our findings reveal that quantum recoil is significant and must be given due consideration even in the nonrelativistic limit, especially when nanoscale and sub-nanoscale periodicities are involved. This is important especially with increasing interest in nanoscale free electron-driven radiation sources, along with the use of low-energy electrons for chip-scale integration [23, 50, 51]. Our theory and experiments focus on spontaneous emission resulting from free electron interaction with the nanometer and sub-nanometer gratings furnished by the periodic lattices of crystalline solids. This is complementary to existing analyses on free electron spontaneous emission using grating periods on the order of 10 nm and larger where the quantum recoil induced photon energy shift is theoretically investigated [39]. Future work includes the study of quantum recoil in the context of related light-matter interactions, such as the inverse Smith-Purcell effect and the inverse Cherenkov effect.

It should be noted that any type of crystalline material – not just van der Waals materials – could have served as the target material in our platform. However, the advantage of using van

der Waals materials arises from the large variety of compound combinations providing precise control over the lattice constants that affect the quantum recoil [52]. To eliminate most electron scattering events in experiments, one can use a target material of thickness less than the electron mean free path (about 10 nm for graphite subjected to ∼10 keV electron energies). Such a small thickness, however, corresponds to a short interaction length could make measuring the Smith-Purcell signal challenging. This could be addressed by increasing the kinetic energy of the electron to increase the mean free path and hence the interaction length.

In summary, our theory and experimental measurements show that quantum recoil in Smith-Purcell radiation can be significant even when driven by conventional table-top electron sources like SEMs and TEMs. We show that table-top electron sources can thus serve as robust, accessible platforms for investigations into quantum aspects of electron-photon interactions. Our experimental findings reveal that quantum recoil is measurable at room temperature and robust to the presence of electron scattering events beyond Smith-Purcell radiation, making it a promising means to precision-tailor the output photon spectra or the post-selected output electron spectra. Prospective applications also include the study of radiation reaction, where crystalline solids have been used for measurements in the regime of ultra-relativistic electron energies [53], and x-ray quantum optics [49].

Acknowledgement

We thank Alan Lim, Yee Yan Tay, and Ido Kaminer for helpful discussions. This project was partially supported by the National Research Foundation (Project ID NRF2020-NRF-ISF004-3525) and the Agency for Science, Technology and Research (A*STAR) Science & Engineering Research Council (Grant No. A1984c0043). We would like to acknowledge the Facility for Analysis, Characterisation, Testing and Simulation, Nanyang Technological University, Singapore, for use of their electron microscopy/x-ray facilities. LJW acknowledges the Nanyang Assistant Professorship Start-up Grant.

Author contributions

SH led the project, designed and performed the electron microscopy experiments and analysed the data. RD and ZL prepared the samples. NP and SH developed the theory and performed the simulations. JSH and CB contributed to the analysis of the experimental results. SH and LJW wrote the paper, with inputs from all other authors. LJW conceived the idea and

supervised the project.

Competing interests

The authors declare no competing interests.

Figure Captions

Fig.1. **Quantum recoil and multimode x-ray generation in Smith-Purcell radiation.** (a) Classically, the electron is assumed to be undeflected for the purposes of determining the emitted photon frequency. This results in uniformly spaced x-ray peaks where the output harmonics are given by $\omega_c = m\omega_0$, where ω_0 is the fundamental frequency. (b) Energy and momentum conservation, however, results in a quantum shift $-\Delta\omega_m$ (which is negative in absolute sign) in the actual output photon energy, resulting in generally non-uniform x-ray peaks at $\omega = \omega_c - \Delta\omega_m$. (c) Experimental measurements of the emitted x-ray spectrum (red) are compared with the results of quantum recoil theory (green), showing excellent agreement. Left and right peaks (labelled "$\hbar\omega_2$" and "$\hbar\omega_4$" respectively) correspond to the $(00\bar{2})$ and $(00\bar{4})$ reciprocal lattice vectors of graphite respectively. The blue curve is the result of classical theory, which neglects quantum recoil. Inset of (c): the coordinate system used in this work. (d) shows the difference $2\hbar\omega_2 - \hbar\omega_4$, where experimental measurements (red) are contrasted against the results of quantum (green) and classical (blue) theory for different electron energies. In all theoretical predictions, electron scattering events beyond Smith-Purcell radiation have been taken into account via Monte Carlo simulations. In (d), the experimental error bars reflect 95% confidence bounds in the Gaussian fitting of the x-ray peaks. The theoretical error bars reflect 95% confidence bounds in the Gaussian fitting of the Monte Carlo simulations, the convergence of the Monte Carlo simulations (relative error $< 10^{-5}$), and the uncertainty of the sample tilt angles (see Methods for details). The experimental results closely favor the predictions of quantum theory over that of classical theory. Our results demonstrate that quantum recoil is measurable on a table-top scale, at room temperature and is robust to the presence of electron scattering events. Inset in (d) shows a scanning electron microscope (SEM) image of the graphite sample (thickness 85 nm) on a transmission electron microscope (TEM) grid, used in the experiments presented here. The sample sizes used to determine the error bars for the peak photon energies experimentally and theoretically are 121 and 1002, respectively. Data are presented as mean values surrounded by error bars denoting the 95% confidence

bounds.

Fig. 2. **Quantum recoil for free electrons interacting with graphite (a-c) and hexagonal boron nitride (d-f).** The x-ray spectra containing the second- and fourth-order Smith-Purcell peaks are shown in each case for different incident electron kinetic energies (labelled). In each panel, the experimental measurements of the x-ray output (red) are compared with theoretical predictions in the presence (green) and absence (blue) of quantum recoil, showing excellent agreement between the experiment and quantum theory.

Fig. 3. **Tuning quantum recoil in Smith-Purcell radiation.** For a given classical emitted photon energy (300 eV in this case, observed at $\theta_{\text{obs}} = 10°$, $\phi_{\text{obs}} = 0°$), the quantum recoil – which directly determines the actual output photon energy – can be tuned by varying the electron energy in combination with the tilt angle; by varying the atomic composition of the crystalline material (different colored lines); or by measuring the emitted photons at different radiation orders (different line styles). The quantum recoil $\hbar\Delta\omega$ is defined as the difference between the classical photon energy and the actual (quantum) photon energy. Exemplary instrumentation corresponding to various ranges of electron energies is listed at the top: scanning electron microscopes (SEM); transmission electron microscopes (TEM); and radiofrequency (RF) gun (still lab-scale). Larger electron energies require additional accelerator stages that result in much larger setups, along with the need for bulky neutron shielding at electron energies > 10 MeV. We see that with existing materials and table-top electron energies, it is possible to achieve actual emitted photon energies from approximately the classical prediction of 300 eV all the way down to extremely low photon energies, by adjusting the amount of quantum recoil. Here $\phi_{\text{til}} = 0°$ and the value of θ_{til} for each point is given in Fig. S13.

References

[1] Frank, I. M. Doppler effect in a refractive medium. *Bull. Russ. Acad. Sci.: Phys.* **6**, 2-2 (1942).

[2] Smith, S. J. & Purcell, E. M. Visible light from localized surface charges moving across a grating. *Phys. Rev.* **92**, 1069 (1953).

[3] Cherenkov, P. A. Visible emission of clean liquids by action of gamma radiation. *Dokl. Akad. Nauk SSSR* **2**, 451–454 (1934).

[4] Tamm, I. E. & Frank, I. M. Coherent visible radiation of fast electrons in a medium. D*okl. Akad. Nauk SSSR* **14**, 107–112 (1937).

[5] Gover, A. et al. Superradiant and stimulated-superradiant emission of bunched electron beams. *Rev. Mod. Phys.* **91**, 035003 (2019).

[6] Polman, A., Kociak, M. & García de Abajo, F. J. Electron-beam spectroscopy for nanophotonics. *Nat. Mater.* **18**, 1158-1171 (2019).

[7] Ryabov, A. & Baum, P. Electron microscopy of electromagnetic waveforms. *Science*, **353**, 374-377 (2016).

[8] Adamo, G. et al. Light well: A tunable free-electron light source on a chip. *Phys. Rev. Lett.* **103**, 113901 (2009).

[9] So, J. K. et al. Cerenkov radiation in metallic metamaterials. *Appl. Phys. Lett.* **97**, 151107 (2010).

[10] Yang, Y. et al. Maximal spontaneous photon emission and energy loss from free electrons. *Nat. Phys.* **14**, 894-899 (2018).

[11] Rivera, N., Wong, L. J., Joannopoulos, J. D., Soljačić, M. & Kaminer, I. Light emission based on nanophotonic vacuum forces. *Nat. Phys.* **15**, 1284-1289 (2019).

[12] Yu, Y. et al. Transition radiation in photonic topological crystals: Quasiresonant excitation of robust edge states by a moving charge. *Phys. Rev. Lett.* **123**, 057402 (2019).

[13] Lin, X. et al. Controlling Cherenkov angles with resonance transition radiation. *Nat. Phys.* **14**, 816-821 (2018).

[14] Lin, X. et al. A Brewster route to Cherenkov detectors. *Nat. Commun.* **2**, 5554 (2021).

[15] Remez, R. et al. Observing the quantum wave nature of free electrons through spontaneous emission. *Phys. Rev. Lett.* **123**, 060401 (2019).

[16] Nussupbekov, A. et al. Enhanced photon emission from free electron excitation of a nanowell. *APL Photonics* **6**, 096101 (2021).

[17] Wang, Z., Yao, K., Chen, M., Chen, H. & Liu, Y. Manipulating Smith-Purcell emission with babinet metasurfaces. *Phys. Rev. Lett.* **117**, 157401 (2016).

[18] Haeusler, U., Seidling, M., Yousefi, P. & Hommelhoff, P. Boosting the Efficiency of Smith–Purcell Radiators Using Nanophotonic Inverse Design. *ACS Photonics* **9**, 664-671 (2022).

[19] Roques-Carmes, C. et al. Free-electron-light interactions in nanophotonics. Preprint at https://doi.org/10.48550/arXiv.2208.02368 (2022).

[20] Ye, Y. et al. Deep-ultraviolet Smith–Purcell radiation. *Optica* **6**, 592-597 (2019).

[21] Shentcis, M. et al. Tunable free-electron X-ray radiation from van der Waals materials. *Nat. Photon.* **14**, 686–692 (2020).

[22] Huang, S. et al. Enhanced Versatility of Table-Top X-Rays from Van der Waals Structures. *Adv. Sci.* 2105401 (2022).

[23] Breuer, J. & Hommelhoff, P. Laser-based acceleration of nonrelativistic electrons at a dielectric structure. *Phys. Rev. Lett.* **111**, 134803 (2013).

[24] Shim, H., Fan, L., Johnson, S. G. & Miller, O. D. Fundamental limits to near-field optical response over any bandwidth. *Phys. Rev. X* **9**, 011043 (2019).

[25] Ginzburg, V. L. Quantum theory of radiation of electron uniformly moving in medium. *Zh. Eksp. Teor. Fiz* **10**, 589-600 (1940).

[26] Neitz, N. & Di Piazza, A. Stochasticity effects in quantum radiation reaction. *Phys. Rev. Lett.* **111**, 054802 (2013).

[27] Debus, A., Steiniger, K., Kling, P., Carmesin, C. M. & Sauerbrey, R. Realizing quantum free-electron lasers: a critical analysis of experimental challenges and theoretical limits. *Phys. Scr.* **94**, 074001 (2019).

[28] Bonifacio, R., Piovella, N., Robb, G. R. M. & Schiavi, A. Quantum regime of free electron lasers starting from noise. *Phys. Rev. ST Accel. Beams* **9**, 090701 (2006).

[29] Baryshevsky, V. G. et al. Experimental observation of frequency tuning of X-ray radiation from nonrelativistic electrons in crystals. *Phys. Lett. A* **363**, 448-452 (2007).

[30] Feranchuk, I. D., Ulyanenkov, A., Harada, J. & Spence, J. C. H. Parametric x-ray radiation and coherent bremsstrahlung from nonrelativistic electrons in crystals. *Phys. Rev. E* **62**, 4225 (2000).

[31] Baryshevsky, V. G. & Feranchuk I. D. The X-ray radiation of ultrarelativistic electrons in a crystal. *Phys. Lett. A* **57**, 183-185 (1976).

[32] Baryshevsky, V. G. & Feranchuk, I. D. Parametric X-rays from ultrarelativistic electrons in a crystal: theory and possibilities of practical utilization. *J. Physique* **44**, 913-922 (1983).

[33] Überall, H. High-energy interference effect of bremsstrahlung and pair production in crystals. *Phys. Rev.* **103**, 1055-1067 (1956).

[34] Tan, Y. J., Pitchappa, P., Wang, N., Singh, R. & Wong, L. J. Space-time wave packets from Smith-Purcell radiation. *Adv. Sci.* 2100925 (2021).

[35] Massuda, A. et al. Smith–Purcell radiation from low-energy electrons. *ACS Photonics* **5**, 3513-3518 (2018).

[36] Talebi, N. Electron-light interactions beyond the adiabatic approximation: recoil engineering and spectral interferometry. *Adv. Phys.: X* **3**, 1499438 (2018).

[37] Barwick, B., Flannigan, D. J. & Zewail, A. H. Photon-induced near-field electron microscopy. *Nature* **462**, 902-906 (2009).

[38] Chahshouri, F., Taleb, M., Diekmann, F. K., Rossnagel, K. & Talebi, N. Interaction of excitons with Cherenkov radiation in WSe_2 beyond the non-recoil approximation. *J. Phys. D: Appl. Phys.* **55**, 145101 (2022)

[39] Tsesses, S., Bartal, G. & Kaminer, I. Light generation via quantum interaction of electrons with periodic nanostructures. *Phys. Rev. A* **95**, 013832 (2017).

[40] Sokolow, A. Quantum theory of Cherenkov effect. *Dokl. Akad. Nauk SSSR* **28**, 415 (1940).

[41] Cox, R. T. Momentum and energy of photon and electron in the Čerenkov radiation. *Phys. Rev.* **66**, 106 (1944).

[42] Kaminer, I. et al. Quantum Čerenkov radiation: spectral cutoffs and the role of spin and orbital angular momentum. *Phys. Rev. X* **6**, 011006 (2016).

[43] Sones, B., Danon, Y. & Block, R. C. X-ray imaging with parametric X-rays (PXR) from a lithium fluoride (LiF) crystal. *Nucl. Instrum. Methods Phys. Res. A* **560**, 589-597 (2006).

[44] Çakmak, G. & Öztürk, T. Continuous synthesis of graphite with tunable interlayer distance. *Diam. Relat. Mater.* **96**, 134-139 (2019).

[45] Roques-Carmes, C., Rivera, N., Joannopoulos, J. D., Soljačić, M. & Kaminer, I. Nonperturbative quantum electrodynamics in the Cherenkov effect. *Phys. Rev. X* **8**, 041013 (2018).

[46] Karnieli, A., Rivera, N., Arie, A. & Kaminer, I. The coherence of light is fundamentally tied to the quantum coherence of the emitting particle. *Sci. Adv.* **7**, eabf8096 (2021).

[47] Pan, Y. & Gover, A. Spontaneous and stimulated radiative emission of modulated free-electron quantum wavepackets-semiclassical analysis. *J. Phys. Commun.* **2**, 115026 (2018).

[48] Wong, L. J. et al. Control of quantum electrodynamical processes by shaping electron wavepackets. *Nat. Commun.* **12**, 1700 (2021).

[49] Wong, L. J. & Kaminer, I. Prospects in X-ray science emerging from quantum optics and nanomaterials. *Appl. Phys. Lett.* **119**, 130502 (2021).

[50] Roques-Carmes, C. et al. Towards integrated tunable all-silicon free-electron light sources. *Nat. Commun.* **10**, 3176 (2019).

[51] Wong, L. J., Kaminer, I., Ilic, O., Joannopoulos, J. D. & Soljačić, M. Towards graphene plasmon-based free-electron infrared to X-ray sources. *Nat. Photon.* **10**, 46-52 (2016).

[52] Geim, A. K. & Grigorieva, I. V. Van der Waals heterostructures. *Nature* **499**, 419-425 (2013).

[53] Wistisen, T. N., Di Piazza, A., Knudsen, H. V. & Uggerhøj, U. I. Experimental evidence of quantum radiation reaction in aligned crystals. *Nat. Commun.* **9**, 795 (2018).

Methods

Monte Carlo simulations: Monte Carlo simulations to capture the impact of electron scattering events beyond Smith-Purcell radiaiton on our measurements were carried out using the CASINO software (details in SI Section S3). Unless otherwise specified, these simulations were performed for both classical theory and quantum theory predictions. The error bars in plots like Fig. 1d capture 95% confidence bounds in the Gaussian fitting of the Monte Carlo simulations, the convergence of the Monte Carlo simulations (relative error $< 10^{-5}$) , and the uncertainty of the sample tilt angle. The convergence of the Monte Carlo simulations were determined by increasing the number of particles used (by 10,000 each time) until the relative change in the output – being the peak photon energy in our case – falls below 10^{-5}. On average, we found that 50,000 particles were needed to achieve convergence in this way. The uncertainty of the sample tilt angle arises from the practical impossibility of exactly determining the tilt angle of the sample in our SEM apparatus. However, we are able to get around this by fitting (method

of least squares) for the tilt angle – which we do separately with classical theory and with quantum theory – not only to obtain the precise value of the tilt angle, but more importantly to see which theory can provide a superior fit to experimental results. As we see in SI Section S7, a much better fit is obtained with quantum theory compared to classical theory. This conclusion continues to be borne out when we apply the best possible fitted angles in classical and quantum scenarios respectively to the classical and quantum theories in Fig. 1d: Once again, the experimental results confirms that the quantum theory is accurate and that we have broken into a regime where quantum recoil is measurable.

Sample preparation: The single-crystal hexagonal boron nitride was synthesized by the atmospheric pressure metal flux method [54]. The hexagonal boron nitride and graphite thin film are exfoliated mechanically onto silicon substrates (with 285 nm SiO_2 film), and transferred to Au grids with the aid of the wet-transfer method. The Au grid is held by a TEM grid holder for SEM during the x-ray measurements in SEM. The benefit of using a TEM grid instead of a regular substrate is that the former minimizes background radiation from free electrons traveling through the sample. The thickness of graphite and hexagonal boron nitride sample used in the Fig. 1 and 2 are 85 ± 2 nm, and 95 ± 2 nm, respectively, which is measured by convergent beam electron diffraction, see SI Section S10 for details.

X-ray measurements: The quantum recoil measurements (Fig. 1 and Figs. 2a-c) were performed in a SEM (EPMA) JEOL JXA-8530F, and the measurements of Figs. 2d-f were performed in FESEM JEOL JSM-7800F PRIME. The emitted x-ray spectra were measured using a silicon drift energy dispersive x-ray spectroscopy detector in the SEM. The x-ray detector was calibrated to measure the x-ray photon energies with an accuracy within $\pm$ 0.5 eV by measuring the Kα peaks of C, N, O, F, Mg, Al and Si (see SI Section S5). The take-off angle $\theta_{\rm obs}$ and the observation angle range $\Delta\theta_{\rm obs}$ are 130° (119°) and 1.67° (11°) for JEOL JXA-8530F (JSM-7800F PRIME), respectively. The energy resolution of the x-ray detector on the JEOL JXA-8530F is $\hbar\Delta\omega_{\rm EDS} \approx 52$ eV (72 eV) for photon energies around 650 eV (1300 eV), and it is $\hbar\Delta\omega_{\rm EDS} \approx 50$ eV (65 eV) for photon energies around 650 eV (1300 eV) for JSM-7800F PRIME. The energy resolution is estimated via measuring the bandwidth of characteristic peaks and interpolating the data in our x-ray photon energy range of interest. The effect of refraction on the x-ray photon exiting the van der Waals crystal is taken into account, as discussed in SI Section S11. Each experimental x-ray spectrum in Figs. 1c and 2a-f was the result of an approximately four-hour measurement. The background radiation of the measured spectra was subtracted using NIST DTSA-II [55, 56]. The overlapped peaks are deconvoluted into separated peaks via multi-Gaussian function fitting, with the 95% confidence bounds of this fitting

reflected in the error bars of plots like Fig. 1d – see SI Section S4 for details.

Data Availability

The data represented in Figs. 1–3 are available as Supplementary information files. All other data that support the plots within this paper and other findings of this study are available from the corresponding author on reasonable request.

Code Availability

All code that support the plots within this paper are available available from the corresponding authors upon reasonable request.

Methods-only references

[54] Liu, S. et al. Single crystal growth of millimeter-sized monoisotopic hexagonal boron nitride. *Chem. Mater.* **30**, 6222-6225 (2018).

[55] Ritchie, N. W. M., Newbury, D. E. & Davis, J. M. EDS measurements of X-ray intensity at WDS precision and accuracy using a silicon drift detector. *Microsc. Microanal.* **18**, 892-904 (2012).

[56] Newbury, D. E. & Ritchie, N. W. M. Performing elemental microanalysis with high accuracy and high precision by scanning electron microscopy/silicon drift detector energy-dispersive X-ray spectrometry (SEM/SDD-EDS). *J. Mater. Sci.* **50**, 493-518 (2015).

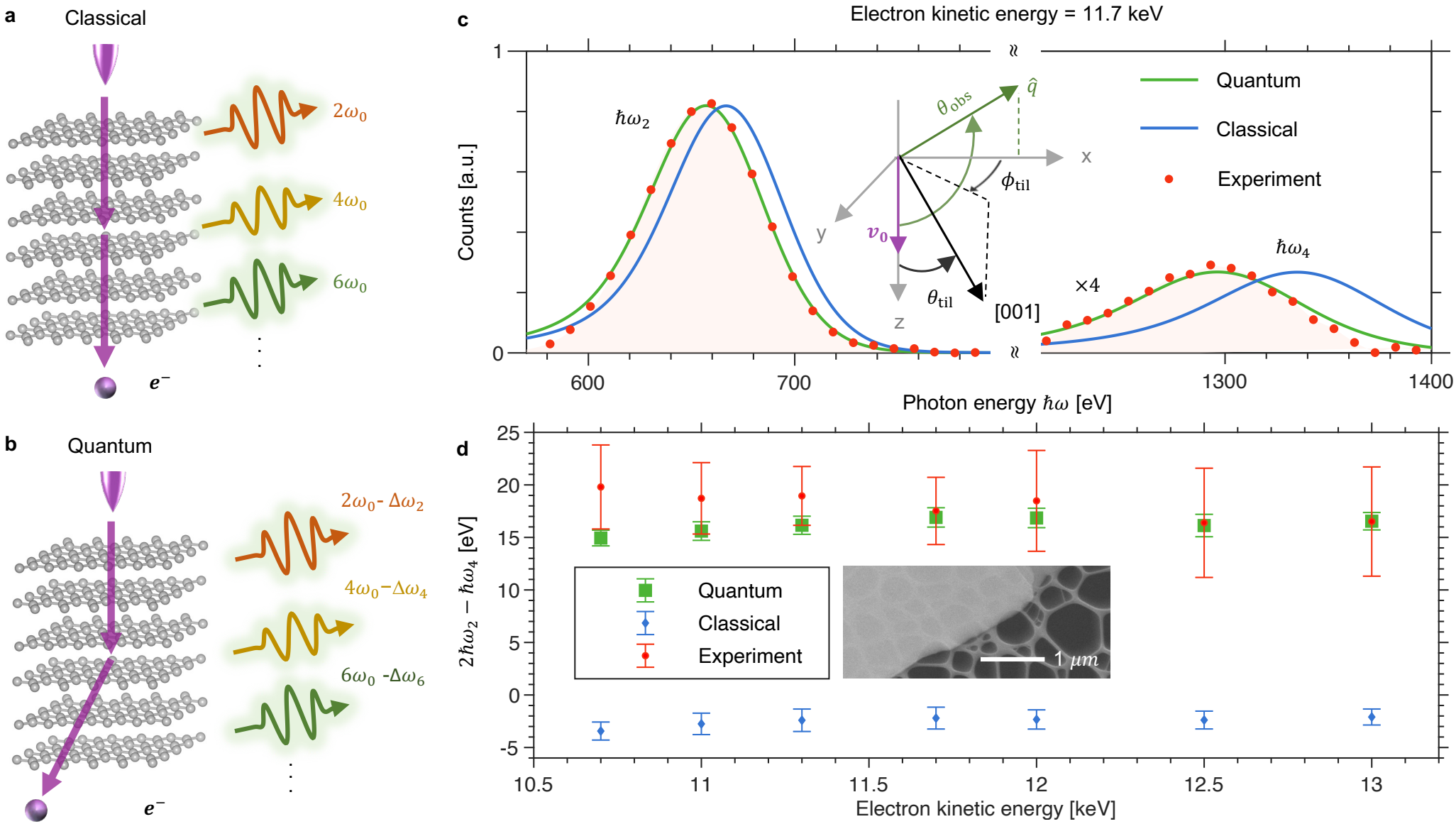
a
Classical
$2\omega_0$
$4\omega_0$
$6\omega_0$
e^-
b
Quantum
$2\omega_0$- $\Delta\omega_2$
$4\omega_0$−$\Delta\omega_4$
$6\omega_0$ -$\Delta\omega_6$
e^-
c
Electron kinetic energy = 11.7 keV
Counts [a.u.]
$\hbar\omega_2$
$\hbar\omega_4$
×4
Quantum
Classical
Experiment
θ_{obs}
$\hat{q}$
x
y
z
ϕ_{til}
θ_{til}
v_0
[001]
Photon energy $\hbar\omega$ [eV]
d
$2\hbar\omega_2 - \hbar\omega_4$ [eV]
Quantum
Classical
Experiment
1 μm
Electron kinetic energy [keV]

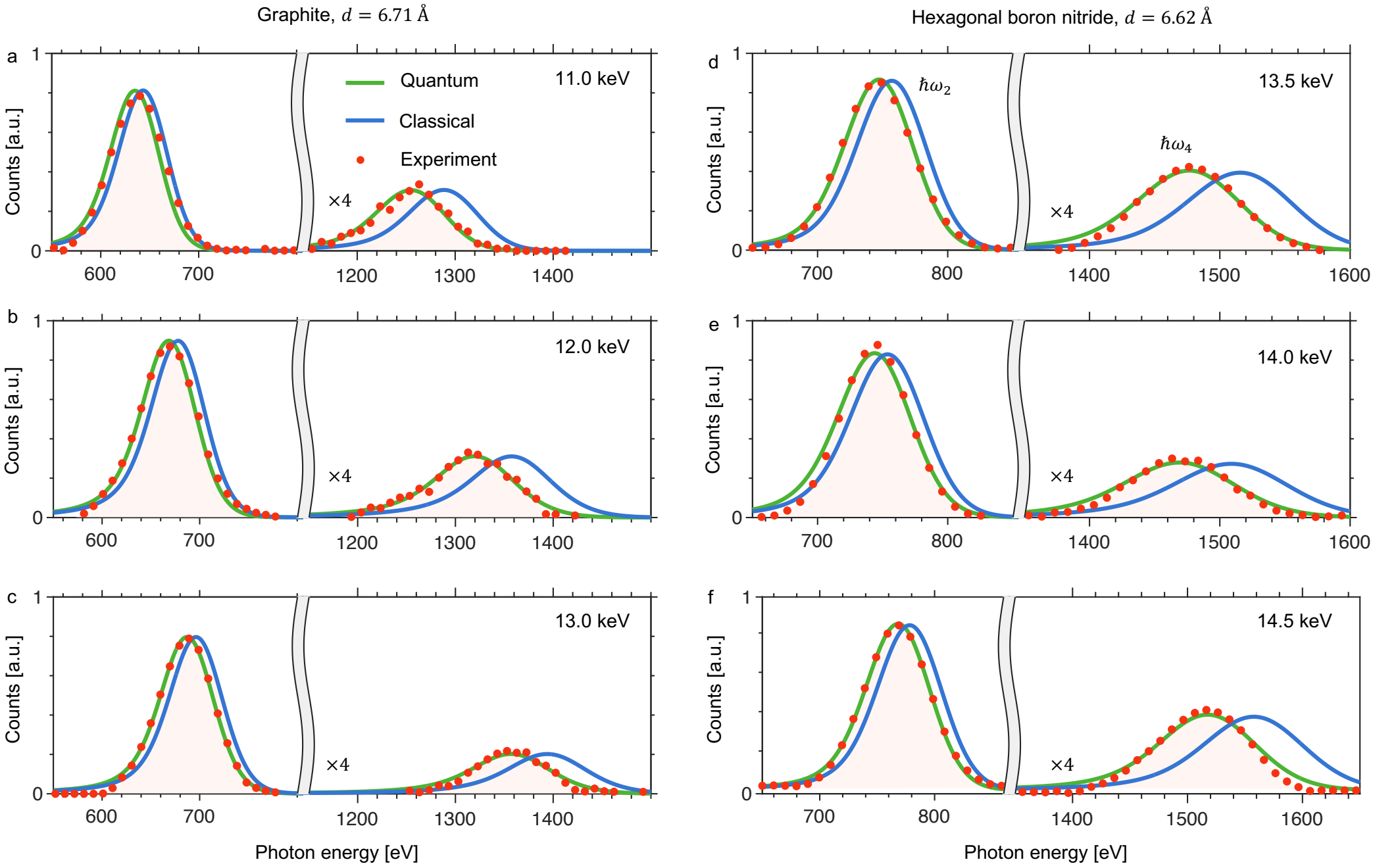
Graphite, $d = 6.71$ Å
Hexagonal boron nitride, $d = 6.62$ Å
a
b
c
d
e
f
Counts [a.u.]
Photon energy [eV]
Quantum
Classical
Experiment
11.0 keV
12.0 keV
13.0 keV
13.5 keV
14.0 keV
14.5 keV
×4
$\hbar\omega_2$
$\hbar\omega_4$

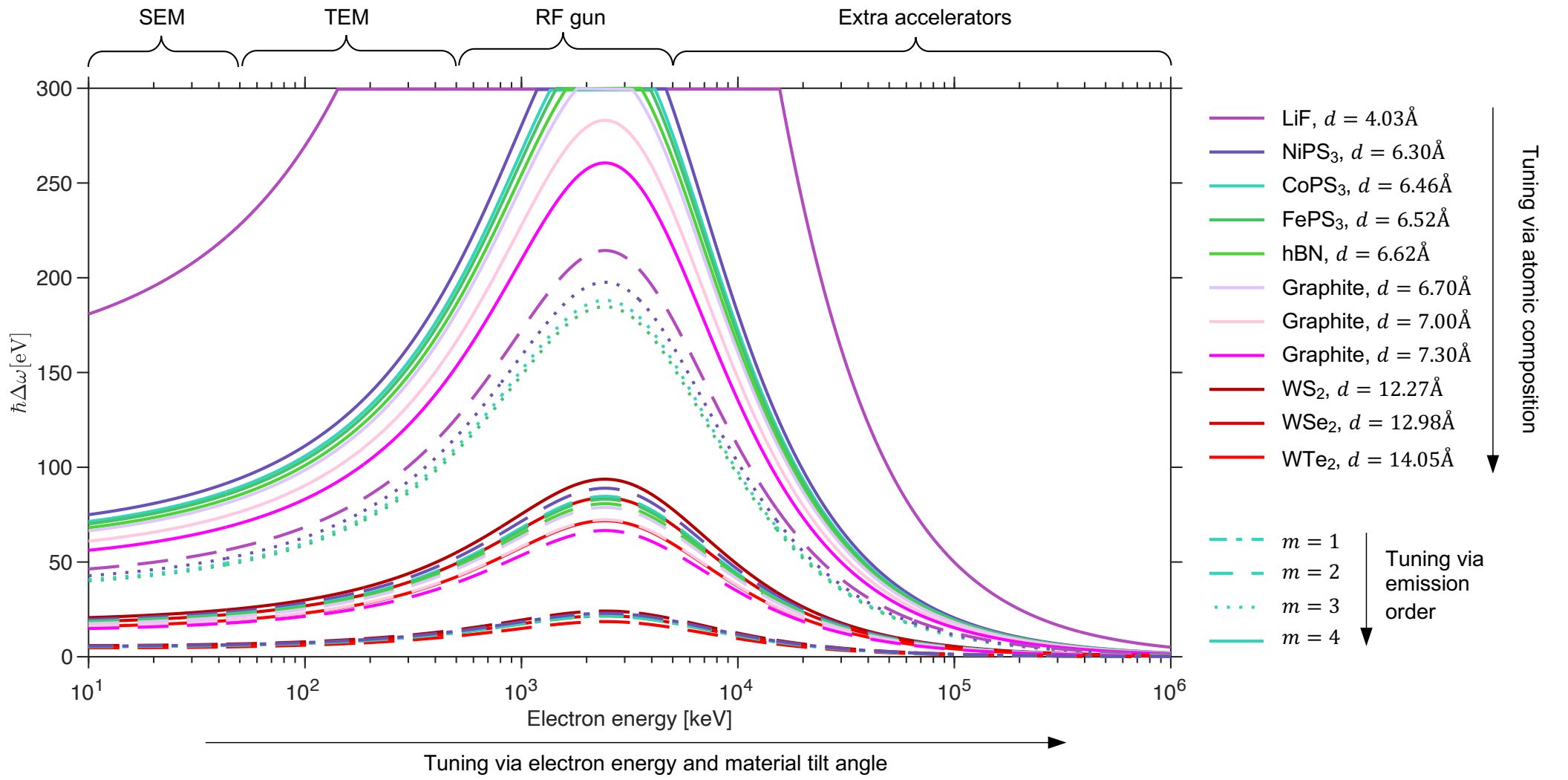
SEM
TEM
RF gun
Extra accelerators
300
250
200
150
100
50
0
$\hbar\Delta\omega$[eV]
10^1
10^2
10^3
10^4
10^5
10^6
Electron energy [keV]
Tuning via electron energy and material tilt angle
LiF, $d = 4.03$Å
$NiPS_3$, $d = 6.30$Å
$CoPS_3$, $d = 6.46$Å
$FePS_3$, $d = 6.52$Å
hBN, $d = 6.62$Å
Graphite, $d = 6.70$Å
Graphite, $d = 7.00$Å
Graphite, $d = 7.30$Å
WS_2, $d = 12.27$Å
WSe_2, $d = 12.98$Å
WTe_2, $d = 14.05$Å
Tuning via atomic composition
$m = 1$
$m = 2$
$m = 3$
$m = 4$
Tuning via emission order